ACS APPLIED MATERIALS & INTERFACES

Research Article

www.acsami.org

Interactive Oxidation−Reduction Reaction for the in Situ Synthesis of Graphene−Phenol Formaldehyde Composites with Enhanced Properties

Xiaojia Zhao,[†] Yang Li,[†] Jinhui Wang,[†] Zhaofei Ouyang,[†] Jingfeng Li,[‡] Gang Wei,*[,‡] and Zhiqiang Su*[,†]

[†]State Key Laboratory of Chemical Resource Engineering, Beijing University of Chemical Technology, 100029 Beijing, China
[‡]Hybrid Materials Interfaces Group, Faculty of Production Engineering, University of Bremen, D-28359 Bremen, Germany

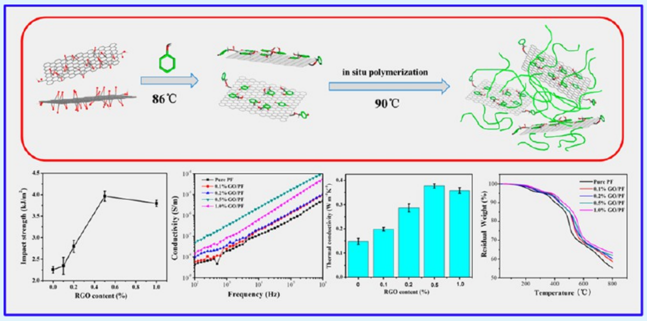

ABSTRACT: We report a facile in situ synthesis of reduced graphene oxide (RGO)−phenol formaldehyde (PF) composites with an interactive oxidation−reduction reaction. In this interactive chemical reaction, graphene oxide (GO) was reduced to RGO by phenol, and simultaneously phenol was oxidized to benzoquinone. The noncovalently adsorbed phenol on the RGO surface can not only serve as an effective reductant but also participate in the in situ polymerization and guide the formation of PF on the RGO surface. RGO−PF composites with different RGO contents were prepared successfully and further characterized with fluorescent spectroscopy, scanning electron microscopy, and transmission electron microscopy. The mechanical strength, electrical conductivity, thermal conductivity, and thermal resistance of the created RGO−PF were investigated. The results indicated that the dispersity of RGO in the PF matrix and the interfacial interaction between RGO and PF were improved greatly because of formation of the RGO−PF hybrid in the in situ synthesis. The homogeneous dispersion and in situ polymerization of RGO sheets help to enhance the thermal conductivity of RGO−PF composites from 0.1477 to 0.3769 W m^{-1} K^{-1} and endow the composites with a good electrical conductivity. In addition, the well-dispersed RGO−PF composites are much more effective in improving their mechanical property and heat resistance.

KEYWORDS: *graphene oxide, oxidation−reduction reaction, phenol formaldehyde, in situ polymerization, property*

■ INTRODUCTION

Graphene, as a single layer of carbon atoms in a hexagonal lattice, has recently attracted much attention.[1,2] Graphene is a potential new material for various applications because of its high thermal conductivity,[3] high mechanical properties,[4,5] and unique electronic characteristics.[6,7] At present, graphene has been prepared by a variety of techniques, including liquid-phase exfoliation of graphite,[8] chemical processing,[9] and thermal treatment.[10] For example, Si and Samulski reported a chemical route to aqueous solutions of isolated graphene sheets by removing residual oxygen functionality and introducing sulfonic acid groups in partially reduced graphene oxide (GO).[11] Chen et al. presented a very simple method to prepare graphene from a GO suspension with the assistance of microwaves in a mixed solution of *N*,*N*-dimethylacetamide and water.[12] Among these methods, chemical reduction of exfoliated GO is an efficient approach to the large-scale production of graphene.[13,14] The common reducing agents of GO include hydrazine,[15−17] strong alkaline,[18] sodium borohydride,[19] and glucose.[20] For example, Gao et al. devised a complete reduction process through chemical conversion by sodium borohydride and sulfuric acid treatment.[21] Ren et al. investigated the reduction effect and mechanism of the as-prepared GO reduced with hydrazine hydrate at different temperatures and time.[22] Although these reducing agents have the remarkable effect of producing highly reduced RGO, some of them, like hydrazine and strong alkaline, are harmful chemicals to both human health and the environment. In addition, several reducing agents may easily enrich the graphene sheets, and it is usually difficult to carry out the purification of graphene. Thus, more environmentally, greener alternatives to the use of such reductants have been highly developed to benefit and facilitate the large-scale production and application of graphene.[23,24] For example, Gao et al. reported an environmentally friendly method to produce graphene that employs Vitamin C as the reductant and amino acid as the stabilizer.[25] This may allow the application of graphene not only for electronic devices but also for biocompatible materials.

Previous studies indicated that the incorporation of graphene with other polymer matrixes can extend the applications of graphene materials. Some polymers like epoxy,[26−28] nylon,[29] poly(methyl methacrylate),[30,31] and polystyrene (PS)[32,33] have been utilized to combine with graphene to create graphene−polymer hybrid materials. To achieve enhanced properties of

Received: December 26, 2013
Accepted: March 3, 2014
Published: March 3, 2014

graphene–polymer materials, the key issue is to obtain well-dispersed graphene with suitable surface modification. However, homogeneous dispersion and interface interaction between graphene and polymer matrixes seem to be the bottlenecks with traditional blending approaches because graphene as a bulk material has a pronounced tendency to agglomerate.[34−37] To solve this problem, two methodologies, namely, the covalent and noncovalent modifications of graphene with polymers, have been carried out.[38−41] The noncovalent modification of graphene was performed by wrapping and adsorbing polymers under the binding force of $\pi-\pi$ interactions. In general, aromatic structures are known to interact strongly with the basal plane of the graphitic surface via $\pi-\pi$ stacking.[38−40] For instance, Shen et al. reported the modification of graphene with PS through $\pi-\pi$ stacking.[40] They found that the PS chains on PS-functional graphene (PSFG) could effectively prevent the aggregation of graphene sheets and the created PS–PSFG composites are homogeneously dispersed and exhibit improved electrical properties. Covalent modification of graphene is performed by GO, which consists of covalently attached oxygenated functional groups such as hydroxyl, epoxy, and carboxyl that made GO easy to disperse in an organic solvent and a polymer matrix. In one typical example, Salavagione et al. reported the covalent modification of graphene sheets with poly(vinyl alcohol) (PVA).[41] They suggested that the covalent linkages between GO and PVA are responsible for the crystallinity and thermal stability of synthesized GO–PVA composites.

Phenol formaldehyde (PF) is preferred in a wide range of applications, from commodity and construction materials to the high-technology aerospace industry. This recognition emerges from the fact that PF has several desirable characteristics, such an high mechanical strength, electrical insulation, flame-retardant resistance, dimensional stability, excellent ablative properties, and low cost.[42−44] On the basis of the excellent performances of PF, its composites have been widely used as a refractory in the field of steel and nonferrous metal smelting,[45] an ablative material in the aerospace industry,[46] braking friction materials in the communications industry,[47] and fire-resistant insulation materials in the construction industry.[48] Especially, to meet the requirements of the ablative materials for aerospace, PF was usually modified by incorporating carbon materials, such as carbon nanofibers, carbon nanotubes, and graphite.[49−51] In spite of the observed thermal stability reinforcing effect, these carbon materials were difficult to disperse in the PF matrix, and thus the expected improvements in thermal resistance and mechanical properties by the incorporation of carbon materials were not fully realized.

In addition, phenol, as a typical monomer of PF, has certain reducibility. We expect that phenol can reduce GO to RGO during in situ polymerization without the addition of other reducing agents, and eventually RGO–PF composites are obtained with excellent performance. In this work, we first proved the reduction ability of phenol on GO and investigated the interactive oxidation–reduction mechanism with the help of a fluorescence spectrophotometer. Then we presented a facile and rapid synthesis of RGO–PF composites by in situ intercalate polymerization with interactive oxidation–reduction of phenol and GO. With the help of transmission electron microscopy (TEM), we investigated the grafting mechanism of RGO–PF composites. The dispersibility of GO in RGO–PF composites was characterized based on microscopic morphologies, and the thermal, electrical, and mechanical properties of RGO–PF composites with different RGO contents were further explored. It was found that good dispersion of RGO and its strong interfacial interaction with the PF matrix are the key factors to improving the properties of the synthesized RGO–PF composites. It is expected that the synthesized RGO–PF composites will have potential applications in thermal interface materials, conductive materials, and other high-technology industries.

EXPERIMENTAL SECTION

Materials. Natural graphite flake (99.8% purity) was obtained from Alfa Aesar. H_2SO_4 (95−98 wt %) and $KMnO_4$ (99.5% purity) were purchased from Beijing Chemical Co., Ltd. (Beijing, China). H_3PO_4 (85% purity) and H_2O_2 (30% aqueous solution) were obtained from Xilong Chemical Co., Ltd. Novolac PF was synthesized in our laboratory with phenol (99%) and formaldehyde (36%) monomers obtained from Beijing Chemical Co., Ltd. (Beijing, China). Oxalic acid (99%), a catalyst agent, was supplied by Beijing Yili Fine Chemical Co., China. Hexamethylenetetramine (HMTA), a curing agent, was supplied by Beijing Yili Fine Chemical Co., China. All chemicals used in this work were of analytical reagent grade and were obtained from commercial sources. The water used was purified through a Millipore system (~18.2 MΩ cm). Carbon-coated copper grids for TEM characterization were purchased from Plano GmbH (Wetzlar, Germany).

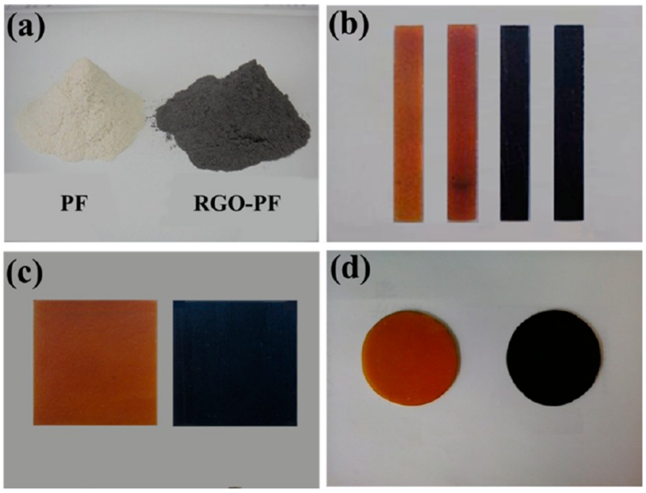

Figure 1. (a) Powder of RGO–PF composites. (b) Specimens for impact tests. (c) Specimens for electrical conductivity tests. (d) Specimens for thermal conductivity tests.

Synthesis of GO. Natural graphite powder was oxidized using a modified method[52] to produce graphite oxide. In brief, a mixture of concentrated H_2SO_4/H_3PO_4 was added to a mixture of graphite flakes (3.0 g), $KMnO_4$, and H_2O_2. Then the mixture was centrifuged, and the remaining solid material was washed in succession with deionized water, 30% HCl, and ethanol. The remaining material was filtered and vacuum-dried overnight at room temperature. Finally, 6.0 g of product was obtained.

Reduction and Noncovalent Modification of GO. The obtained GO was suspended in water (0.5 mg mL^{-1}) and exfoliated through ultrasonication for 2 h to obtain homogeneous GO dispersion. Then 7.5 g of phenol was added into 150 mL of the homogeneous GO dispersion, followed by stirring for 2.5 h at 86 °C. Finally, the resulting stable black dispersion was centrifuged (15000 rpm) and washed with water three times. The final products were obtained after remaining in vacuum freeze drying for 2 days.

Interactive Oxidation–Reduction Reaction and in Situ Polymerization for the Creation of RGO–PF Composites. The detailed reaction process is as follows. The reagents 300 g of phenol,

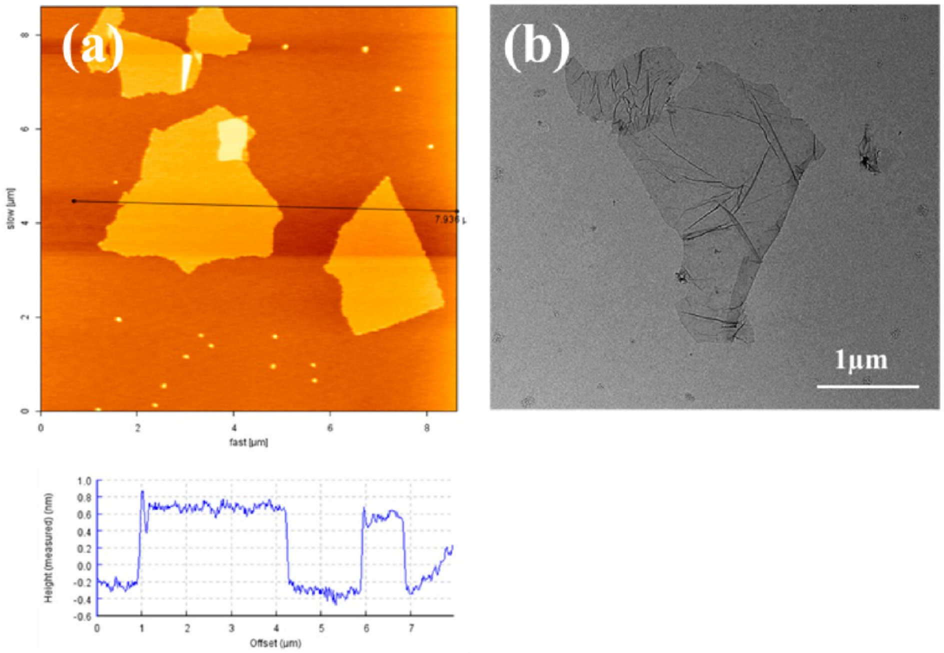

Figure 2. Structure characterization of GO: (a) AFM height image; (b) TEM image.

162 g of formaldehyde (36 wt % water solution), and 1.5 g of oxalic acid were fed into the three-neck flask reactor, and the reaction proceeded at 86 °C. Simultaneously, GO solutions with different contents (0, 0.1, 0.2, 0.5, and 1.0 wt %, respectively) were treated with a bath sonicator (100 W and 40 kHz) for 60 min. Then the solutions were dropwise added into the reaction system. After the reaction proceeded at 86 °C for 60 min, 52 g of formaldehyde and 0.9 g of oxalic acid were replenished to the system and further reacted at 90 °C for another 90 min. Finally, the reaction product was dehydrated at a Gauge pressure of −0.1 MPa until the temperature reached 150 °C.

Characterization Techniques. Fourier transform infrared spectroscopy (FT-IR; Nicolet 6700, Thermo-Fisher Scientific Inc., Waltham, MA), X-ray diffraction (XRD; Rigaku D/max-2500 VB +PC), Raman spectroscopy (LabRAM, Horiba JY, Edison, NJ), and X-ray photoelectron spectroscopy (XPS; ESCALAB 250) were used to compare the structures of GO and RGO. Atomic force microscopy (AFM) images were recorded using a NanoWizard 3 NanoScience atomic force microscope (JPK Instruments AG, Berlin, Germany) in tapping mode to identify the thickness of the GO sheets. A fluorescence spectrophotometer (PE-LS-55, America) was used to detect the products during the process of reduction of GO. TEM experiments were performed on a Tecnai $G^2$20 transmission electron microscope (FET) with an accelerating voltage of 200 kV, RGO sheets were dispersed in ethanol by sonication for 15 min, and some pieces were collected on carbon-coated 200-mesh copper grids for TEM observation. For RGO−PF composites, the reaction solution in the late stage of polymerization was added to alcohol to dissolve PF, and precipitates were directly disposed with vacuum freeze drying after high-speed centrifugation. Then the precipitates were dissolved in alcohol and dropped on carbon-coated copper grids for TEM observation. The dispersion of RGO in the PF matrix was verified by scanning electron microscopy (SEM; JSM-6700F).

Property Tests of RGO−PF Composites. RGO−PF composite powders mixed with 10% HMTA were poured into molds with different dimensions, and the molds put into a press-molding machine (model SLY-812A, Dongguan Blue Eagle Jewelry Machinery Factory) for curing. A four-step curing procedure was used: from room temperature to 110 °C for 30 min under a pressure of 2−3 MPa and then slow increasing pressure 12 MPa and increasing temperature to 170 °C within 30 min. After that, the pressure and temperature of the system were maintained for 10 min. Then the system was cooled naturally to 50 °C, while the pressure was kept at 12 MPa. At last, we obtained various test samples according to the different molds, as shown in Figure 1.

Mechanical Property. To characterize the mechanical behavior of the specimens (80 mm × 10 mm × 4 mm), the IZOD test was performed using a GT-7054-1 impact machine (Gotech testing machines). A tensile test was conducted using a Gotech TCS-2000 tensile tester. At least five specimens were tested for each sample.

Electrical Conductivity. The electrical conductivities of RGO−PF composites were measured by an Agilent 4294A instrument. The specimen dimensions were 10 mm × 10 mm × 2 mm. In order to provide stable values of the resistivity, the samples were coated with a layer of silver to ensure good electrical contact. All of the conductivity measurements were carried out at room temperature.

Thermal Conductivity. The thermal conductivities of RGO−PF composites were measured by a through-plane thermal conductivity analyzer (HC-074, Japan) at room temperature. The samples with 60.0 mm iameter and 2.0 mm thickness were tightly pressed between two parallel plates, which have a certain temperature difference.

Thermal Resistance. The heat decomposition temperature (T_d) and ablative resistance were measured by thermogravimetric analysis (TGA) with a TGA Q500 thermal analyzer at a heating rate of 10 °C min^{-1} from 20 to 800 °C in an atmosphere of nitrogen.

RESULTS AND DISCUSSION

Interactive Oxidation−Reduction Mechanism of GO and Phenol. An improved synthesis method was utilized to prepare GO.[52] Compared to the Hummers method, this new method does not generate toxic gas and the temperature is easily controlled. Moreover, the improved method yields a higher fraction of well-oxidized hydrophilic carbon material and GO possesses a more regular structure.[53] To investigate the morphology of the synthesized GO, AFM and TEM have been utilized. The representative AFM image of the GO sheet in Figure 2a exhibits that the measured thickness of the GO sheet is 1.0 nm, which agrees with the previous reports on the thickness of a single layer of the GO sheet.[54,55] TEM was further used to confirm the nanosheet morphology of GO, and the curly layer morphology of GO sheets is clearly shown (Figure 2b).

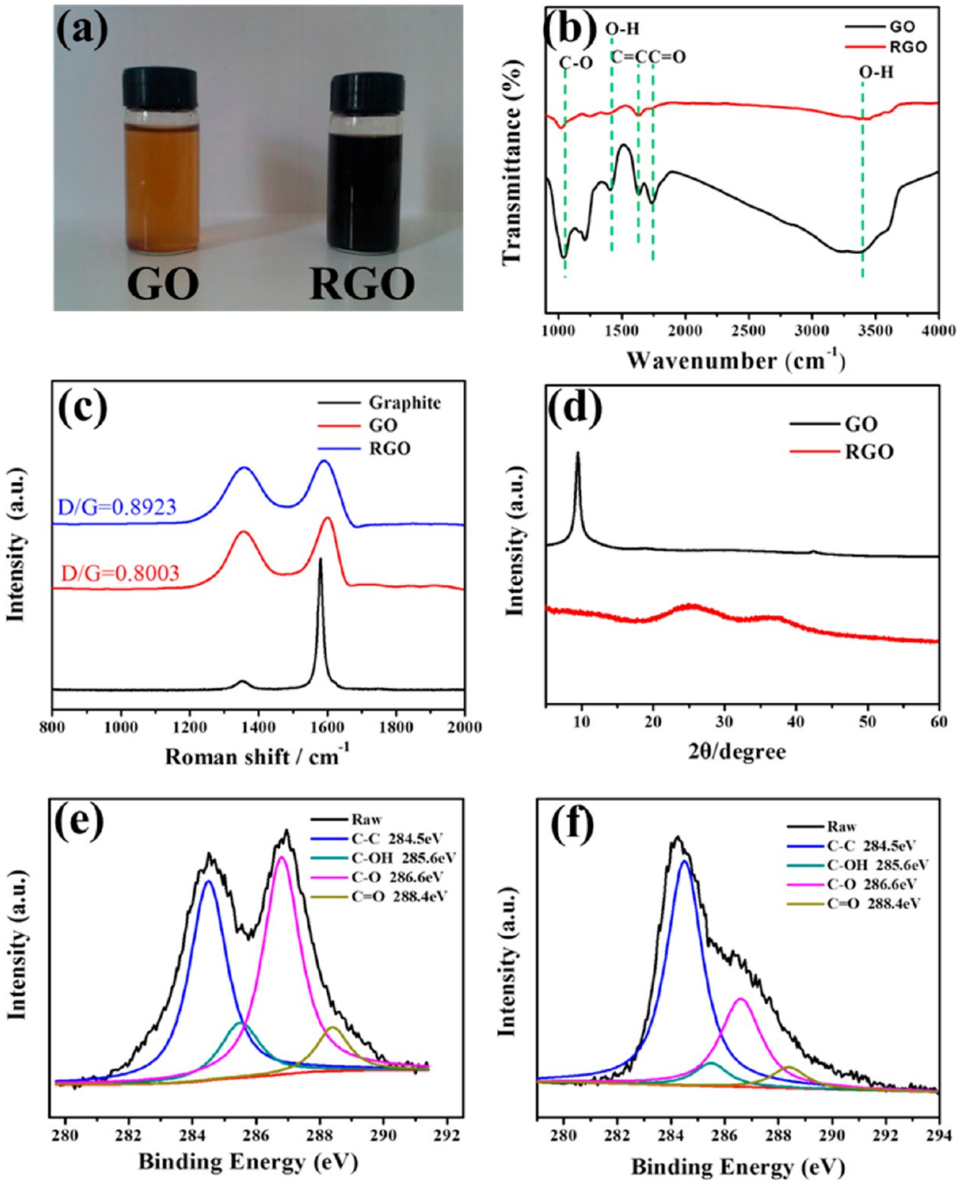

Figure 3. Characterizations of GO and phenol-reduced RGO: (a) photographs; (b) FT-IR spectra; (c) Raman spectra; (d) XRD spectra; C 1s XPS spectra of GO (e) and RGO (f).

To confirm the interactive oxidation−reduction of phenol and GO in this system, first we characterize GO before and after reduction by phenol. Figure 3a shows the photographs of GO and a phenol-reduced RGO solution. It can be clear found that the color changes from yellow to black after phenol reduction, which proved the successful formation of RGO. Figure 3b presents the FT-IR spectra of GO and RGO. The spectrum of GO shows several absorption peaks at 3403 and 1405 cm^{-1} (OH), 1733 cm^{-1} (C=O stretching), 1622 cm^{-1} (C=C), and 1060 cm^{-1} (CO).[56] For the created RGO, the characteristic absorption peaks of oxide groups (OH, C=O, and CO) were found to decrease dramatically, indicating that GO has been reduced to RGO. Figure 3c gives the Raman spectra of GO and RGO. Two peaks at about 1363 and 1594 cm^{-1} can be assigned to the D and G bands, respectively. The D band is related to the vibrations of sp^3 carbon atoms of disordered graphene nanosheets, and the G band corresponds to the vibrations of sp^2 carbon atom domains of graphite.[55] Similar to that reported for GO,[55] the G band (1594 cm^{-1}) broadens after oxidation with the appearance of the D band at 1363 cm^{-1}. In Figure 3c, it was found that I_D/I_G increases from 0.80 to 0.89 after reduction, indicating that most of the oxygenated groups would have been removed during the reduction process.[57]

Power XRD was further used to characterize GO and RGO, and the typical patterns are shown in Figure 3d. The feature diffraction peak of GO appearing at 9.50° (d spacing ∼9.32 Å) was observed as a result of the introduction of oxygenated functional groups on the carbon sheets.[15] For the obtained RGO, the peak located at 9.5° disappears and shows a dramatic shift to higher 2θ angles (25.10°; d spacing ∼3.54 Å), confirming the successful reduction of GO to RGO and the possible exfoliation of the multilayered RGO.[58]

To further identify the formation of RGO, XPS was performed to characterize removal of the oxygen groups. Figure 3e shows the C 1s spectrum of GO. Four different peaks centered at 284.5, 285.6, 286.6, and 288.4 eV are observed, corresponding to C=C in aromatic rings and C−OH, C−O,

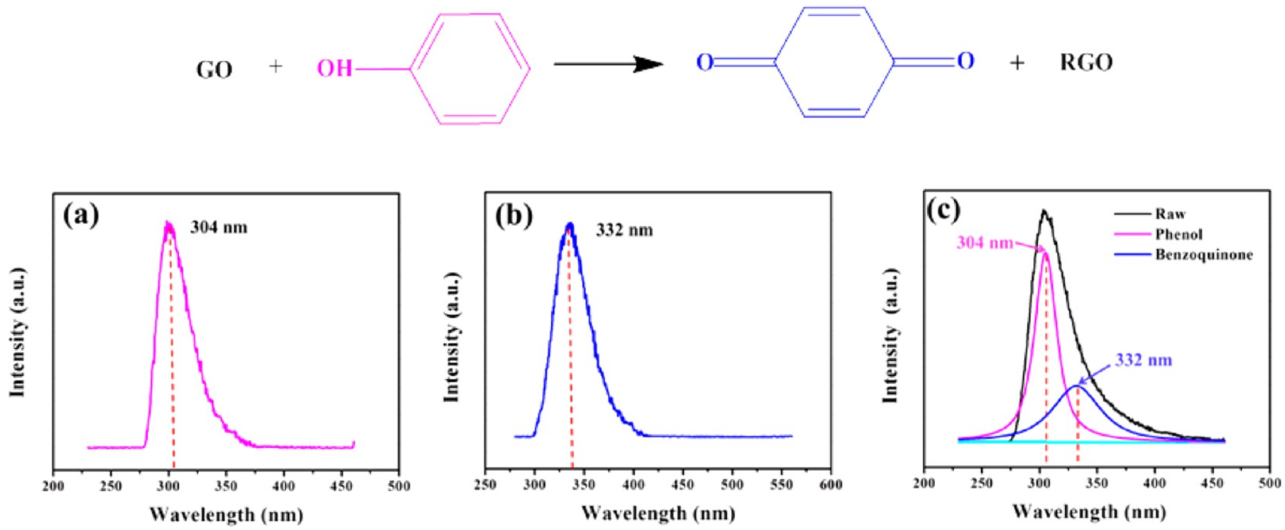

Figure 4. Fluorescence spectra of (a) phenol, (b) benzoquinone, and (c) the oxidation product.

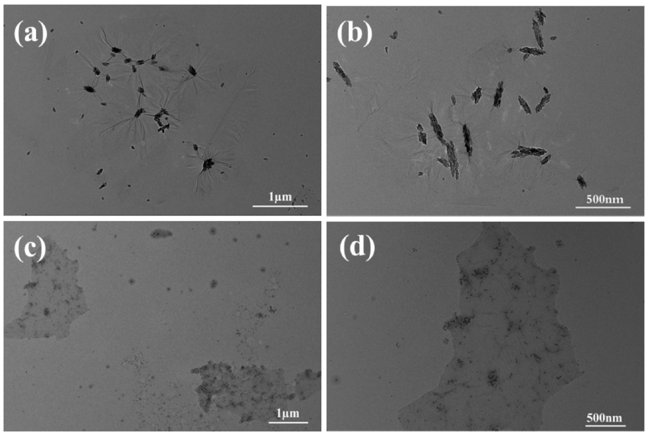

Figure 5. Typical TEM images of (a and b) a RGO−phenol hybrid before polymerization and (c and d) RGO−PF extracted from composites.

and C═O groups, respectively. For RGO shown in Figure 3f, the intensities of all C 1s peaks of the carbon binding to oxygen, especially the peak of C−O, decreased dramatically, indicating that most of the oxygen-containing functional groups were removed after reduction. In addition, the O/C atomic ratios of GO and RGO declined obviously from 47.45% to 29.50%, which gave a clearer indication of the extent of reduction achieved.

On basis of the above results, we proposed a potential interactive oxidation−reduction mechanism of the GO−phenol system, as shown in Figure 4. We suggest that phenol promotes the remove of oxygen functional groups of GO and the formation of RGO; at the same time, the GO oxidizes phenol to benzoquinone. In a previous report, Wang et al. reported the reduction of GO with hydroquinone.[59] Hydroquinone acted as a reducing agent by losing either one H^+ from one of its hydroxyls to form a monophenolate ion or two H^+ from both hydroxyls to form a diphenolate ion (quinone). To test our hypothesis, we further utilized fluorescence spectroscopy to characterize phenol and the oxidation product, and the corresponding florescence spectra are shown in Figure 4a−c. Detailed analysis of the fluorescence spectra provides clear evidence on the above hypothesis. The spectra of phenol (Figure 4a) and benzoquinone (Figure 4b) show characteristic peaks at 304 and 332 nm, respectively. Figure 4c shows the fluorescence spectra of the oxidation product; the major peaks at 304 and 332 nm indicate the presence of phenol and benzoquinone. Despite the fact that the intensity peak of benzoquinone is relatively weak, it provides clear evidence of the existence of benzoquinone.

In Situ Polymerization of PF on RGO. Parts a and b of Figure 5 show the typical TEM images of RGO−phenol hybrids before in situ polymerization. It can be found that a lot of substances were enriched by the surface folding of RGO sheets, which were extrapolated to phenol and benzoquinone via analysis of the interactive oxidation−reduction mechanism of GO and phenol. It is suggested that phenol and phenol homologues adsorb on both sides of the GO sheets via a $\pi-\pi$ stacking interaction, which provides the amount of active sites for propagation of the PF chains. As a result, the PF chains gradually grafted onto the GO sheets in the condensation reaction.

According to the "grafting" strategy, the interfacial interaction between RGO sheets and the PF matrix was enhanced, immensely improving their compatibility. Moreover, the high density of grafting could help to reduce aggregation of the nanoscale RGO sheets.[60]

The schematic illustration of the formation of RGO−PF composites is shown in Figure 6. At a certain temperature, monomers were initiated by oxalic acid to conduct condensation polymerization (Figure 6a). Simultaneously, a GO solution was added to the initial reaction system of PF (Figure 6b), and the interactive oxidation−reduction reaction between phenol and GO was started. The phenol and phenol homologues, like benzoquinone and (hydroxymethyl)phenol, were enriched on GO sheets through noncovalent interaction via $\pi-\pi$ stacking, as shown in Figure 6c. In addition, the ester bonds were formed through the reaction between the carboxy group on the edge of the GO sheets and the hydroxymethyl groups of (hydroxymethyl)phenol (Figure 6c). Because there are many active points on the GO sheets, with the consumption of monomers, the PF chains gradually propagated and grew onto the GO sheets by a condensation reaction (Figure 6d).

In order to further verify this proposed mechanism, the created RGO-PF composites after in situ polymerization were

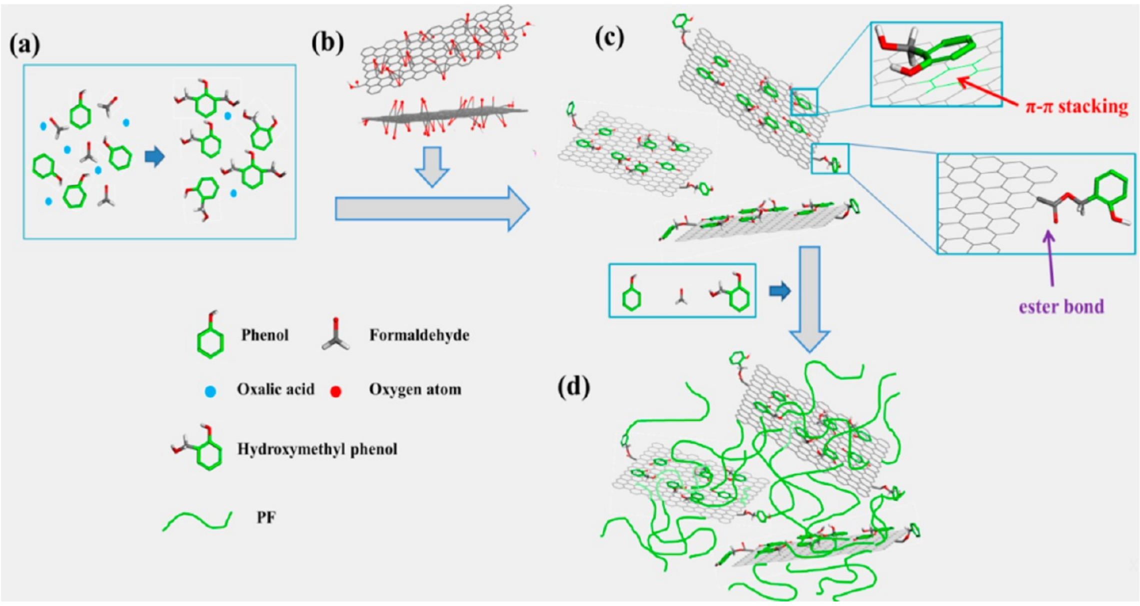

Figure 6. Schematic illustration of the formation of RGO−PF composites: (a) initial reaction system of PF; (b) GO solution added to the initial reaction system; (c) interactive oxidation−reduction of GO and phenol; (d) in situ polymerization.

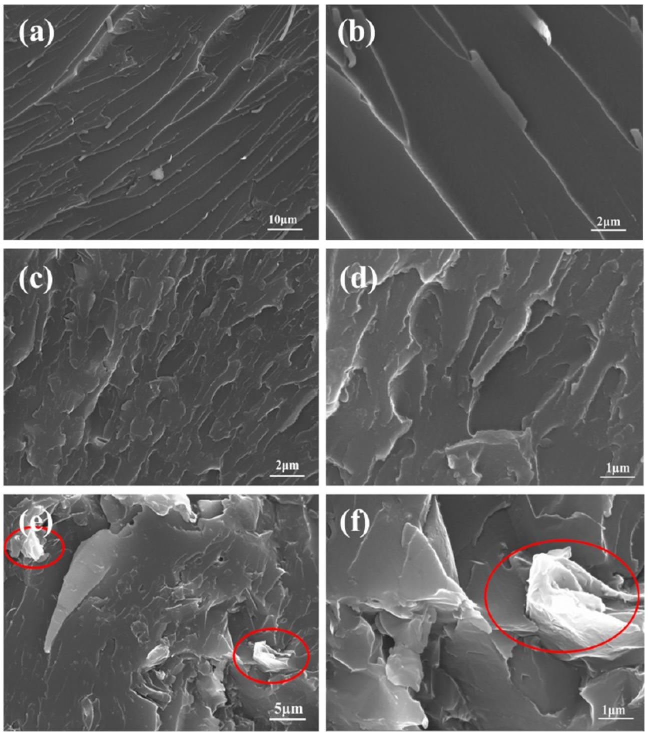

Figure 7. SEM photographs of the impact fracture surface of RGO−PF composites: (a and b) untoughened; (c and d) 0.5 wt % RGO content; (e and f) 1.0 wt % RGO content.

characterized. Figure 5c and 5d show the typical TEM images of RGO-PF in reaction solution in the late stage of polymerization. Based on the TEM result, we could inspect the typical stretched and wrapped patterns of graphene sheets which were well-distributed without congregation. The resultant homogeneous dispersion of graphene sheets in composites provided the utmost element to obtain superior performances of composites. In addition, the PF-grafted graphene sheets could be observed clearly. The PF was well-distributed on the surface of graphene sheets ascribing to the high density of grafting, which provides good places for the polymer to grow, as shown in Figure 6d.

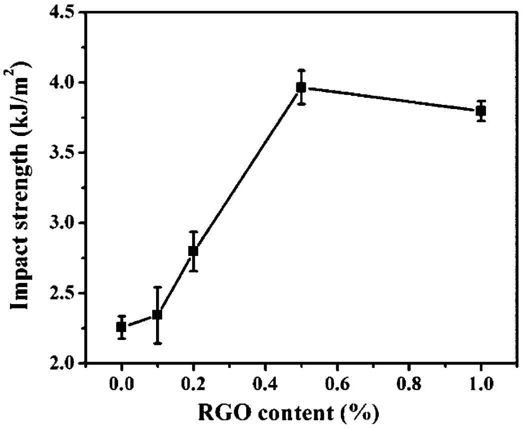

Figure 8. Impact strength of RGO−PF composites with different RGO contents.

Structural Characterization of RGO−PF Composites. Figure 7 shows the morphology of fractured surfaces of RGO−PF composites, which exhibit compatibility and dispersion of RGO in PF. As shown in Figure 7a,b, the fracture surface of neat PF is very smooth, indicating typical brittle fracture characteristics and revealing its nature of weak resistance to crack initiation and propagation.[61] In the case of the composite with 0.5 wt % RGO, the fracture surface exhibits a rougher fracture surface (Figure 7c,d), and numerous wrinkles can be observed, which indicates good compatibility between RGO and PF as well as good dispersion of RGO in PF. We suggest that two main factors are responsible for this. The first factor, immensely good compatibility, was attributed to the $\pi-\pi$ stacking interactions between RGO and PF, which provide suitable sites for polymer to grow on the RGO sheets. The second factor is that the PF chains grafted on the RGO sheets have relatively uniform length, which thickened most of the RGO sheets with similar extent.[62] Thus, the propagating PF

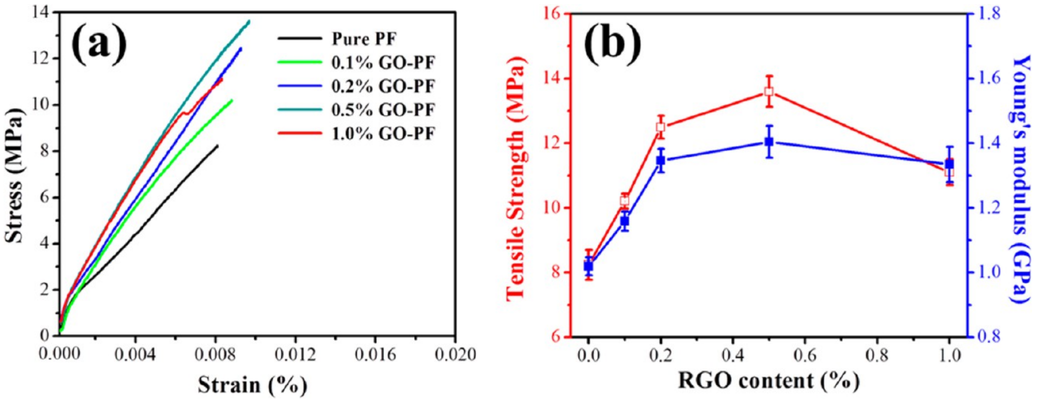

Figure 9. (a) Typical stress−strain curves of RGO−PF composites with different RGO contents. (b) Tensile strength and Young's modulus changes with increasing graphene content.

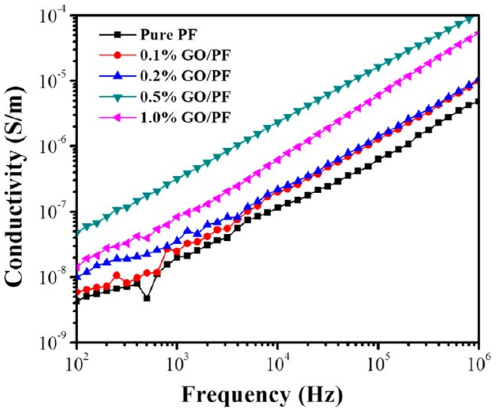

Figure 10. log−log plot of the conductivity with respect to the frequency for RGO−PF composites with different RGO contents.

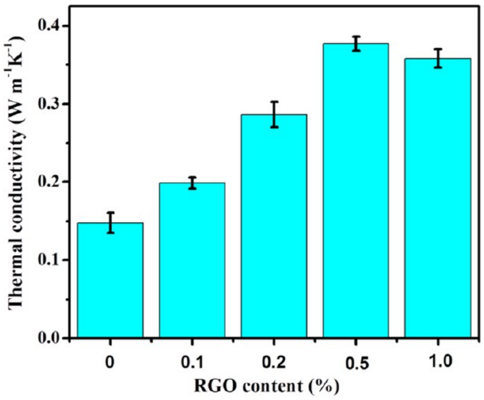

Figure 11. Thermal conductivity of RGO−PF composites with different RGO contents.

chains reduced the aggregation of RGO sheets. Comparatively, the RGO−PF composite with higher loading (1.0 wt % RGO) exhibits insufficient dispersion (Figure 7e,f). Although the fracture surface is relatively rough with some wrinkles, it should be noted that the RGO sheets dispersed in PF exist in the form of agglomerates (see the red marks in the figures).

Mechanical Strength. Figure 8 shows the impact strength of RGO−PF composites with different RGO contents, and it is found that the impact strength is enhanced with an increase of the RGO content. When the RGO content increases to 0.5 wt %, the increase of the impact strength is particularly significant. It is surprising that the impact strength begins to decrease when the content of RGO was increased to 1.0 wt %. We suggest that this phenomenon is ascribed to the aggregation of RGO sheets. The RGO agglomerates would form steric obstacles, causing bad interlocking with the host resin matrix and restraining energy dissipation during the fracture process. In turn, good dispersion of the GO sheets in composites could lead to an increase in energy dissipation during the fracture process.[63]

Figure 9a shows typical experimental stress−strain curves of RGO−PF composites with different RGO contents. Figure 9b shows the average tensile strength and Young's modulus for RGO−PF composites. The tensile strength of RGO−PF composites increased from 23.91% to 65.09% with 0.1−0.5 wt % RGO. However, for RGO−PF composites with 1.0 wt % RGO, an obvious decrease of the tensile strength was observed. For specimens with 0.1−0.5 wt % RGO, Young's modulus of RGO−PF composites increased from 13.74% to 37.78% and no further increase of Young's modulus was observed for specimens with 1.0 wt % RGO. Such tensile properties of RGO−PF composites could be attributed to efficient load transfer between RGO sheets and the PF matrix. As mentioned before, the existence of $\pi-\pi$ stacking between RGO and PF endowed RGO with good compatibility. In addition, it would also affect the tensile strength of composites. When the content of RGO was increased to 1.0 wt %, poor dispersion and interface interaction were presumably responsible for the tensile performance improvement. Therefore, the composite with 0.5 wt % RGO exhibits a better tensile property for good dispersion of the RGO sheets and the rich interface interaction between RGO and PF.

It should be noted that the mechanical properties of RGO−PF composites strongly depend on the extent of load transfer between RGO and the PF matrix, which is closely bound with the microstructure of the synthesized composites.

Electrical Conductivity. Figure 10 presents the log−log plot of the conductivity with respect to frequency at room temperature for RGO−PF with different RGO contents. It can be seen that the conductivity of composites continues to increase with an increase of the frequency. In addition, the conductivity of RGO−PF composites with different RGO contents shows a corresponding increase with 0.1−0.5 wt % RGO. As shown in Figure 10, the conductivity of PF with 0.5 wt % RGO is nearly 1 order of magnitude higher in comparison to that of a pure PF composite. However, for RGO−PF composites with 1.0 wt % RGO, its conductivity shows a decreasing trend.

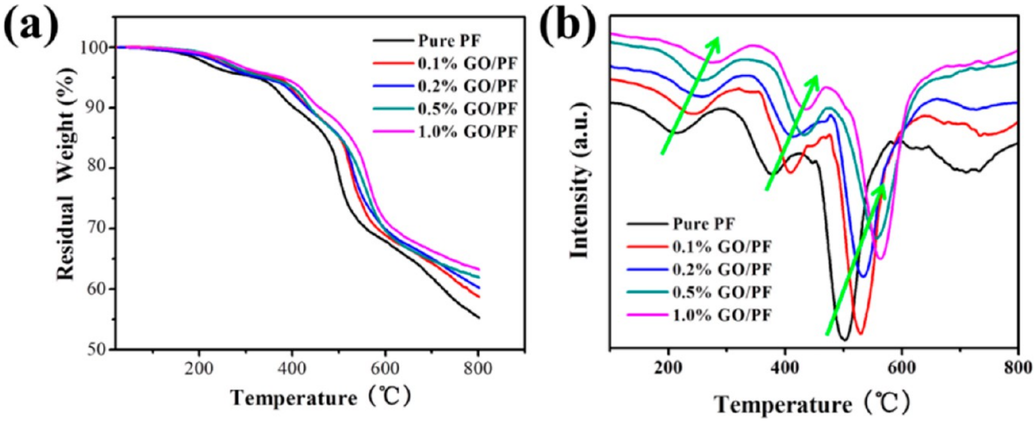

Figure 12. Thermal resistance of RGO−PF composites with different RGO contents: (a) TG and (b) DTG curves.

It is well established that the electrical properties of polymer composites with fillers depend on properties such as the dispersion state, filler geometry, and filler−filler interaction.[64] In our work, the geometry and interaction of conductive RGO are almost the same. Therefore, the dispersion level of RGO is crucial to determining the final electrical properties of RGO−PF composites. Good dispersion of RGO sheets in the PF matrix can promote the formation of an effective network for electron path transmittance.[65] Thus, the RGO−PF composite with 0.5 wt % RGO exhibits the highest electrical conductivity attributed to the homogeneous dispersion of RGO.

Moreover, the electrical conductivity may also have a connection with the arrangement and orientation of RGO sheets in the matrix. In a previous report, Ding et al. found that RGO sheets were mostly vertical to the cross section of composites and the randomly distributed platelike RGO sheets in the matrix tend to align parallel to the hot pressing plane.[62] We suggest that the homogeneous dispersion and ordered arrangement of RGO sheets in the RGO−PF composites can favor the formation of consecutive electrical conductive pathways or networks.

Thermal Conductivity. Figure 11 displays the thermal conductivity of RGO−PF composites. It can be found that the thermal conductivity increased consistently with an increase of the RGO loading, which is similar to the tendency of the electrical conductivity with different RGO contents. The thermal conductivity of the RGO−PF composites with 0.5 wt % RGO loading increased by 155%, referring to that of neat PF (from 0.1477 to 0.3769 W m^{-1} K^{-1}). Equally, the composite with higher-loading 1.0 wt % RGO exhibits relatively low thermal conductivity.

Usually, the changing pattern of thermal conductivity is corresponding to that of the electrical conductivity, and the analysis about the electrical conductivity can also be used to explain the thermal conductivity. According to the previous report, the thermal energy is transferred mainly in the form of phonons in composite.[66] Therefore, the good coupling in vibration modes at the filler−polymer interface will be in favor of reducing the generation of significant interface thermal resistance. The chemical bonding between the filler and matrix can efficiently reduce the acoustic phonon scattering at the interface.[3] In our work, the PF chains were chemically grafted onto RGO sheets through π−π stacking interactions and the ester bond. RGO−PF composites own good thermal conductivity, which has wide potential applications in the high-performance thermal management systems, such as the computer industry, auto industry, and so on.

Thermal Resistance. Figure 12 shows the TGA and differenetial thermal analysis (DTA) curves of RGO−PF composites with different RGO contents. The weight changes of different RGO−PF composites can be clearly recognized from the TGA curves (Figure 12a). The percentage of weight reduction at 800 °C indicates the carbon residual value after the RGO−PF composites were degraded. In Figure 12a, it is obvious that neat PF has the lowest carbon residual value (55.25%) and RGO−PF composites have a higher carbon residue consistent with an increase of the RGO loading; the highest carbon residual weight could reach 63.25% (1.0 wt % GO). Compared with other polymers, PF has a higher carbon residual value and has been widely used as an ablation-resistant material especially in the aerospace field.[67] In our work, it was found that only a 1.0 wt % addition of GO could enhance the carbon residual value of neat PF by 8% and endow PF composites better heat resistance. We suggest that this might be caused by two factors. First, graphene, as a kind of carbon material, has a certain contribution to the increase of the carbon yield. However, such a contribution should be very small because the fraction of RGO in the composites is at most 1 wt %. Second, in our opinion, in the in situ intercalate polymerization, PF chains grown on the surface of RGO sheets exhibit a better regularity and crystallinity, which is the main reason for making an invaluable contribution to the improvement of the ablative resistance.

Figure 12b shows the typical DTA curves of RGO−PF composites with different RGO contents. The peaks shown in the DTA curves correspond to the decomposition temperature of different constituents in the composites. In the temperature range of 150−450 °C, the weights of the composites have a certain loss, which may be attributed to the inadequate curing resin with the loss of small molecules. In addition, the temperatures corresponding to the maximum mass loss for the RGO−PF composites with different RGO contents (0%, 0.1%, 0.2%, 0.5%, and 1.0%) have been recorded, corresponding to 500.15, 525.56, 532.21, 556.73, and 562.72 °C, respectively. It can be observed that the decomposition temperature increased consistently with an increase of the RGO loading, which indicates that RGO improved the thermal decomposition temperature of PF composites to a great extent.

CONCLUSIONS

In the present work, the RGO−PF composites with an interactive oxidation−reduction reaction were synthesized by in situ intercalate polymerization. In this chemical reaction, GO was reduced to RGO by phenol, and simultaneously phenol was oxidized to benzoquinone. The noncovalently adsorbed phenol on the RGO surface can not only serve as an effective reductant but also participate in in situ polymerization and guide the formation of PF on the RGO surface. Furthermore, because of noncovalent interaction via $\pi-\pi$ stacking and covalent bonding between GO and phenol homologues, GO sheets have good dispersion and strong interfacial interactions with the PF matrix. As a result, the created RGO−PF composites exhibit enhanced performances on the mechanical strength, electrical conductivity, thermal conductivity, and thermal resistance. We expect that the novel RGO−PF composites will have wide applications in aerospace, communications, and construction industries.

AUTHOR INFORMATION

Corresponding Authors

*E-mail: wei@uni-bremen.de.
*E-mail: suzq@mail.buct.edu.cn.

Notes

The authors declare no competing financial interest.

ACKNOWLEDGMENTS

We acknowledge financial support from the Fundamental Research Funds for the Central Universities (Project ZZ1307). We thank the German Academic Exchange Council for a short-term scholarship and the China Scholarship Council for a Ph.D. scholarship.

REFERENCES

(1) Novoselov, K. S.; Geim, A. K.; Morozov, S. V.; Jiang, D.; Zhang, Y.; Dubonos, S. V.; Grigorieva, I. V.; Firsov, A. A. Electric Field Effect in Atomically Thin Carbon Films. *Science* **2004**, *306*, 666−669.

(2) Geim, A. K.; Novoselov, K. S. The Rise of Graphene. *Nat. Mater.* **2007**, *6*, 183−191.

(3) Balandin, A. A.; Ghosh, S.; Bao, W.; Calizo, L.; Teweldebrhan, D.; Miao, F.; Lau, C. N. Superior Thermal Conductivity of Single-Layer Graphene. *Nano Lett.* **2008**, *8*, 902−907.

(4) Rafiee, M. A.; Rafiee, J.; Wang, Z.; Song, H.; Yu, Z. Z.; Koratkar, N. Enhanced Mechanical Properties of Nanocomposites at Low Graphene Content. *ACS Nano* **2009**, *3*, 3884−3890.

(5) Park, S.; Lee, K. S.; Bozoklu, G.; Cai, W. W.; Nguyen, S. T.; Ruoff, R. S. Graphene Oxide Papers Modified by Divalent Ions—Enhancing Mechanical Properties via Chemical Cross-Linking. *ACS Nano* **2008**, *2*, 572−578.

(6) Novoselov, K. S.; Geim, A. K.; Morozov, S. V.; Jiang, D.; Katsnelson, M. I.; Grigorieva, I. V.; Dubonos, S. V.; Firsov, A. A. Two-Dimensional Gas of Massless Dirac Fermions in Graphene. *Nature* **2005**, *438*, 197−200.

(7) Kopelevich, Y.; Esquinazi, P. Graphene Physics in Graphite. *Adv. Mater.* **2007**, *19*, 4559−4563.

(8) Bourlinos, A. B.; Georgakilas, V.; Zboril, R.; Steriotis, T. A.; Stubos, A. K. Liquid-Phase Exfoliation of Graphite towards Solubilized Graphenes. *Small* **2009**, *5*, 1841−1845.

(9) Wang, H.; Robinson, J. T.; Li, X.; Dai, H. Solvothermal Reduction of Chemically Exfoliated Graphene Sheets. *J. Am. Chem. Soc.* **2009**, *131*, 9910−9911.

(10) McAllister, M. J.; Li, J. L.; Adamson, D. H.; Schniepp, H. C.; Abdala, A. A.; Liu, J.; Herrera-Alonso, M.; Milius, D. L.; Car, R.; Prud'homme, R. K.; Aksay, L. A. Single Sheet Functionalized Graphene by Oxidation and Thermal Expansion of Graphite. *Chem. Mater.* **2007**, *19*, 4396−4404.

(11) Si, Y.; Samulski, E. T. Synthesis of Water Soluble Graphene. *Nano Lett.* **2008**, *8*, 1679−1682.

(12) Chen, W.; Yan, L.; Bangal, P. R. Preparation of Graphene by the Rapid and Mild Thermal Reduction of Graphene Oxide Induced by Microwaves. *Carbon* **2010**, *48*, 1146−1152.

(13) Xu, Y.; Liu, Z.; Zhang, X.; Wang, Y.; Tian, J.; Huang, Y.; Ma, Y.; Zhang, X.; Chen, Y. A Graphene Hybrid Material Covalently Functionalized with Porphyrin: Synthesis and Optical Limiting Property. *Adv. Mater.* **2009**, *21*, 1275−1279.

(14) Bai, H.; Xu, Y.; Zhao, L.; Li, C.; Shi, G. Non-Covalent Functionalization of Graphene Sheets by Sulfonated Polyaniline. *Chem. Commun.* **2009**, 1667−1669.

(15) Gao, X.; Jang, J.; Nagase, S. Hydrazine and Thermal Reduction of Graphene Oxide: Reaction Mechanisms, Product Structures, and Reaction Design. *J. Phys. Chem. C* **2009**, *114*, 832−842.

(16) Park, S.; An, J.; Potts, J. R.; Velamakanni, A.; Murali, S.; Ruoff, R. S. Hydrazine-Reduction of Graphite and Graphene Oxide. *Carbon* **2011**, *49*, 3019−3023.

(17) Park, S.; An, J.; Jung, I.; Piner, R. D.; An, S. J.; Li, X.; Velamakanni, A.; Ruoff, R. S. Colloidal Suspensions of Highly Reduced Graphene Oxide in a Wide Variety of Organic Solvents. *Nano Lett.* **2009**, *9*, 1593−1597.

(18) Fan, X.; Peng, W.; Li, Y.; Li, X.; Wang, S.; Zhang, G.; Zhang, F. Deoxygenation of Exfoliated Graphite Oxide under Alkaline Conditions: A Green Route to Graphene Preparation. *Adv. Mater.* **2008**, *20*, 4490−4493.

(19) Shin, H. J.; Kim, K. K.; Benayad, A.; Yoon, S. M.; Park, H. K.; Jung, I. S.; Jin, M. H.; Jeong, H. K.; Kim, J. M.; Choi, J. Y.; Lee, Y. H. Efficient Reduction of Graphite Oxide by Sodium Borohydride and Its Effect on Electrical Conductance. *Adv. Funct. Mater.* **2009**, *19*, 1987−1992.

(20) Wei, G.; Zhang, Y.; Steckbeck, S.; Su, Z.; Li, Z. Biomimetic Graphene−FePt Nanohybrids with High Solubility, Ferromagnetism, Fluorescence, and Enhanced Electrocatalytic Activity. *J. Mater. Chem.* **2012**, *22*, 17190−17195.

(21) Gao, W.; Alemany, L. B.; Ci, L.; Ajayan, P. M. New Insights into the Structure and Reduction of Graphite Oxide. *Nat. Chem.* **2009**, *1*, 403−408.

(22) Ren, P. G.; Yan, D. X.; Ji, X.; Chen, T.; Li, Z. M. Temperature Dependence of Graphene Oxide Reduced by Hydrazine Hydrate. *Nanotechnology* **2011**, *22*, 055705.

(23) Paredes, J. I.; Villar-Rodil, S.; Fernández-Merino, M. J.; Guardia, L.; Martínez-Alonso, A.; Tascón, J. M. D. Environmentally Friendly Approaches toward the Mass Production of Processable Graphene from Graphite Oxide. *J. Mater. Chem.* **2011**, *21*, 298−306.

(24) Fernández-Merino, M. J.; Villar-Rodil, S.; Paredes, J. I.; Solís-Fernández, P.; Guardia, L.; García, R.; Martínez-Alonso, A.; Tascon, J. M. D. Identifying Efficient Natural Bioreductants for the Preparation of Graphene and Graphene−Metal Nanoparticle Hybrids with Enhanced Catalytic Activity from Graphite Oxide. *Carbon* **2013**, *63*, 30−44.

(25) Gao, J.; Liu, F.; Liu, Y.; Ma, N.; Wang, Z. Q.; Zhang, X. Environment-Friendly Method to Produce Graphene that Employs Vitamin C and Amino Acid. *Chem. Mater.* **2010**, *22*, 2213−2218.

(26) Liang, J.; Wang, Y.; Huang, Y.; Ma, Y.; Liu, Z.; Cai, J.; Zhang, C.; Gao, H.; Chen, Y. Electromagnetic Interference Shielding of Graphene/Epoxy Composites. *Carbon* **2009**, *47*, 922−925.

(27) Teng, C. C.; Ma, C. C. M.; Lu, C. H.; Yang, S. Y.; Lee, S. H.; Hsiao, M. C.; Yen, M. Y.; Chiou, K. C.; Lee, T. M. Thermal Conductivity and Structure of Non-Covalent Functionalized Graphene/Epoxy Composites. *Carbon* **2011**, *49*, 5107−5116.

(28) Kim, J.; lm, H.; Kim, J.; Kim, J. Thermal and Electrical Conductivity of $Al(OH)_3$ Covered Graphene Oxide Nanosheet/Epoxy Composites. *J. Mater. Sci.* **2012**, *47*, 1418−1426.

(29) Rafiq, R.; Cai, D.; Jin, J.; Song, M. Increasing the Toughness of Nylon 12 by the Incorporation of Functionalized Graphene. *Carbon* **2010**, *48*, 4309−4314.

(30) Zhang, H. B.; Zheng, W. G.; Yan, Q.; Jiang, Z. G.; Yu, Z. Z. The Effect of Surface Chemistry of Graphene on Rheological and Electrical Properties of Polymethylmethacrylate Composites. *Carbon* **2012**, *50*, 5117−5125.

(31) Villar-Rodil, S.; Paredes, J. I.; Martínez-Alonso, A.; Tascón, J. M. D. Preparation of Graphene Dispersions and Graphene−Polymer Composites in Organic Media. *J. Mater. Chem.* **2009**, *19*, 3591−3593.

(32) Sun, S.; Cao, Y.; Feng, J.; Wu, P. Click Chemistry as a Route for the Immobilization of Well-Defined Polystyrene onto Graphene Sheets. *J. Mater. Chem.* **2010**, *20*, 5605−5607.

(33) Yan, D. X.; Ren, P. G.; Pang, H.; Fu, Q.; Yang, M. B.; Li, Z. M. Efficient Electromagnetic Interference Shielding of Lightweight Graphene/Polystyrene Composite. *J. Mater. Chem.* **2012**, *22*, 18772−18774.

(34) Stankovich, S.; Dikin, D. A.; Piner, R. D.; Kohlhaas, K. A.; Kleinhammes, A.; Jia, Y. Y.; Wu, Y.; Nguyen, S. T.; Ruoff, R. S. Synthesis of Graphene-Based Nanosheets via Chemical Reduction of Exfoliated Graphite Oxide. *Carbon* **2007**, *45*, 1558−1565.

(35) Li, D.; Müller, M. B.; Gilje, S.; Kaner, R. B.; Wallace, G. G. Processable Aqueous Dispersions of Graphene Nanosheets. *Nat. Nanotechnol.* **2008**, *3*, 101−105.

(36) Stankovich, S.; Dikin, D. A.; Dommett, G. H. B.; Kohlhaas, K. M.; Zimney, E. J.; Stach, E. A.; Piner, R. D.; Nguyen, S. T.; Ruoff, R. S. Graphene-Based Composite Materials. *Nature* **2006**, *442*, 282−286.

(37) Chen, R. J.; Zhang, Y.; Wang, D.; Dai, H. Noncovalent Sidewall Functionalization of Single-Walled Carbon Nanotubes for Protein Immobilization. *J. Am. Chem. Soc.* **2001**, *123*, 3838−3839.

(38) Björk, J.; Hanke, F.; Palma, C. A.; Samori, P.; Cecchini, M.; Persson, M. Adsorption of Aromatic and Anti-Aromatic Systems on Graphene through π−π Stacking. *J. Phys. Chem. Lett.* **2010**, *1*, 3407−3412.

(39) Zhang, X.; Feng, Y.; Tang, S.; Fang, W. Preparation of a Graphene Oxide−Phthalocyanine Hybrid through Strong π−π Interactions. *Carbon* **2010**, *48*, 211−216.

(40) Shen, B.; Zhai, W.; Chen, C.; Lu, D.; Wang, J.; Zheng, W. Melt Blending In situ Enhances the Interaction between Polystyrene and Graphene through π−π Stacking. *ACS Appl. Mater. Interfaces* **2011**, *3*, 3103−3109.

(41) Salavagione, H. J.; Gómez, M. A.; Martínez, G. Polymeric Modification of Graphene through Esterification of Graphite Oxide and Poly(vinyl alcohol). *Macromolecules* **2009**, *42*, 6331−6334.

(42) Park, J. K.; Cho, D.; Kang, T. J. A Comparison of the Interfacial, Thermal, and Ablative Properties between Spun and Filament Yarn Type Carbon Fabric/Phenolic Composites. *Carbon* **2004**, *42*, 795−804.

(43) Sreejith, P. S.; Krishnamurthy, R.; Malhotra, S. K.; Narayanasamy, K. Evaluation of PCD Tool Performance during Machining of Carbon/Phenolic Ablative Composites. *J. Mater. Process. Technol.* **2000**, *104*, 53−58.

(44) Park, J. K.; Kang, T. J. Thermal and Ablative Properties of Low Temperature Carbon Fiber−Phenol Formaldehyde Resin Composites. *Carbon* **2002**, *40*, 2125−2134.

(45) Hashemi, B.; Nemati, Z. A.; Faghihi-Sani, M. A. Effects of Resin and Graphite Content on Density and Oxidation Behavior of MgO−C Refractory Bricks. *Ceram. Int.* **2006**, *32*, 313−319.

(46) Natali, M.; Monti, M.; Puglia, D.; Kenny, J. M.; Torre, L. Ablative Properties of Carbon Black and MWNT/Phenolic Composites: A Comparative Study. *Composites, Part A* **2012**, *43*, 174−182.

(47) Hong, U. S.; Jung, S. L.; Cho, K. H.; Cho, M. H.; Kim, S. J.; Jang, H. Wear Mechanism of Multiphase Friction Materials with Different Phenolic Resin Matrices. *Wear* **2009**, *266*, 739−744.

(48) Chiu, H. T.; Chiu, S. H.; Jeng, R. E.; Chung, J. S. A Study of the Combustion and Fire-Retardance Behavior of Unsaturated Polyester/Phenolic Resin Blends. *Polym. Degrad. Stab.* **2000**, *70*, 505−514.

(49) Yoonessi, M.; Toghiani, H.; Wheeler, R.; Porcar, L.; Kline, S.; Pittman, C. U., Jr. Neutron Scattering, Electron Microscopy and Dynamic Mechanical Studies of Carbon Nanofiber/Phenolic Resin Composites. *Carbon* **2008**, *46*, 577−588.

(50) Kim, S. J.; Jang, H. Friction and Wear of Friction Materials Containing Two Different Phenolic Resins Reinforced with Aramid Pulp. *Tribol. Int.* **2000**, *33*, 477−484.

(51) Bafekrpour, E.; Simon, G. P.; Yang, C.; Chipara, M.; Habsuda, J.; Fox, B. A Novel Carbon Nanofibre/Phenolic Nanocomposites Coated Polymer System for Tailoring Thermal Behavior. *Composites, Part A* **2013**, *46*, 80−88.

(52) Marcano, D. C.; Kosynkin, D. V.; Berlin, J. M.; Sinitskii, A.; Sun, Z.; Slesarev, A.; Alemany, L. B.; Lu, W.; Tour, J. M. Improved Synthesis of Graphene Oxide. *ACS Nano* **2010**, *4*, 4806−4814.

(53) Higginbotham, A. L.; Kosynkin, D. V.; Sinitskii, A.; Sun, Z.; Tour, J. M. Lower-Defect Graphene Oxide Nanoribbons from Multiwalled Carbon Nanotubes. *ACS Nano* **2010**, *4*, 2059−2069.

(54) Wang, H.; Sun, D.; Zhao, N.; Yang, X.; Shi, Y.; Li, J.; Su, Z.; Wei, G. Thermo-Sensitive Graphene Oxide−Polymer Nanoparticle Hybrids: Synthesis, Characterization, Biocompatibility and Drug Delivery. *J. Mater. Chem. B* **2014**, *2*, 1362−1370.

(55) Zhang, P.; Zhang, X.; Zhang, S.; Lu, X.; Li, Q.; Su, Z.; Wei, G. One-Pot Green Synthesis, Characterizations, and Biosensor Application of Self-Assembled Reduced Graphene Oxide−Gold Nanoparticle Hybrid Membranes. *J. Mater. Chem. B* **2013**, *1*, 6525−6531.

(56) Moon, I. K.; Lee, J.; Ruoff, R. S.; Lee, H. Reduced Graphene Oxide by Chemical Graphitization. *Nat. Commun.* **2010**, *1*, 73−79.

(57) Zhong, X.; Jin, J.; Li, S.; Niu, Z.; Hu, W.; Li, R.; Ma, J. Aryne Cycloaddition: Highly Efficient Chemical Modification of Graphene. *Chem. Commun.* **2010**, *46*, 7340−7342.

(58) Hassan, H. M. A.; Abdelsayed, V.; Abd El Rahman, S. K.; AbouZeid, K. M.; Terner, J.; El-Shall, M. S.; Al-Resayes, S. I.; El-Azhary, A. A. Microwave Synthesis of Graphene Sheets Supporting Metal Nanocrystals in Aqueous and Organic Media. *J. Mater. Chem.* **2009**, *19*, 3832−3837.

(59) Wang, G.; Yang, J.; Park, J.; Gou, X.; Wang, B.; Liu, H.; Yao, J. Facile Synthesis and Characterization of Graphene Nanosheets. *J. Phys. Chem. C* **2008**, *112*, 8192−8195.

(60) Xu, Z.; Gao, C. In situ Polymerization Approach to Graphene-Reinforced Nylon-6 Composites. *Macromolecules* **2010**, *43*, 6716−6723.

(61) Yu, Z.; Li, J.; Yang, L.; Yao, Y.; Su, Z.; Chen, X. Synthesis and Properties of Nano Carboxylic Acrylonitrile Butadiene Rubber Latex Toughened Phenolic Resin. *J. Appl. Polym. Sci.* **2012**, *123*, 1079−1084.

(62) Ding, P.; Su, S.; Song, N.; Tang, S.; Liu, Y.; Shi, L. Highly Thermal Conductive Composites with Polyamide-6 Covalently-Grafted Graphene by an In Situ Polymerization and Thermal Reduction Process. *Carbon* **2014**, *66*, 576−584.

(63) Tang, L. C.; Wan, Y. J.; Yan, D.; Pei, Y. B.; Zhao, L.; Li, Y. B.; Wu, L. B.; Jiang, J. X.; Lai, G. Q. The Effect of Graphene Dispersion on the Mechanical Properties of Graphene/Epoxy Composites. *Carbon* **2013**, *60*, 16−27.

(64) Song, Y. S.; Youn, J. R. Influence of Dispersion States of Carbon Nanotubes on Physical Properties of Epoxy Nanocomposites. *Carbon* **2005**, *43*, 1378−1385.

(65) Zaman, I.; Kuan, H. C.; Dai, J.; Kawashima, N.; Michelmore, A.; Sovi, A.; Dong, S.; Luong, L.; Ma, J. From Carbon Nanotubes and Silicate Layers to Graphene Platelets for Polymer Nanocomposites. *Nanoscale* **2012**, *4*, 4578−4586.

(66) Zhong, H.; Lukes, J. R. Interfacial Thermal Resistance between Carbon Nanotubes: Molecular Dynamics Simulations and Analytical Thermal Modeling. *Phys. Rev. B* **2006**, *74*, 125403.

(67) Bianchi, D.; Turchi, A.; Nasuti, F.; Onofri, M. Chemical Erosion of Carbon−Phenolic Rocket Nozzles with Finite-Rate Surface Chemistry. *J. Propul. Power* **2013**, *29*, 1220−1230.